Eur. J. Biochem. **271**, 3399–3413 (2004) © FEBS 2004 doi:10.1111/j.1432-1033.2004.04274.x

NMR and molecular dynamics studies of an autoimmune myelin basic protein peptide and its antagonist

Structural implications for the MHC II (I-A^u)–peptide complex from docking calculations

Andreas G. Tzakos[1], Patrick Fuchs[2], Nico A. J. van Nuland[2], Anastasios Troganis[3], Theodore Tselios[4], Spyros Deraos[4], John Matsoukas[4], Ioannis P. Gerothanassis[1] and Alexandre M. J. J. Bonvin[2]

[1]*Department of Chemistry, Section of Organic Chemistry and Biochemistry, University of Ioannina, Greece;* [2]*Bijvoet Center for Biomolecular Research, Department of NMR Spectroscopy, Utrecht, the Netherlands;* [3]*Department of Biological Applications and Technologies, University of Ioannina, Greece;* [4]*Department of Chemistry, University of Patras, Greece*

Experimental autoimmune encephalomyelitis can be induced in susceptible animals by immunodominant determinants of myelin basic protein (MBP). To characterize the molecular features of antigenic sites important for designing experimental autoimmune encephalomyelitis suppressing molecules, we report structural studies, based on NMR experimental data in conjunction with molecular dynamic simulations, of the potent linear dodecapeptide epitope of guinea pig MBP, Gln74-Lys75-Ser76-Gln77-Arg78-Ser79-Gln80-Asp81-Glu82-Asn83-Pro84-Val85 [MBP(74–85)], and its antagonist analogue Ala81MBP(74–85). The two peptides were studied in both water and Me_2SO in order to mimic solvent-dependent structural changes in MBP. The agonist MBP(74–85) adopts a compact conformation because of electrostatic interactions of Arg78 with the side chains of Asp81 and Glu82. Arg78 is 'locked' in a well-defined conformation, perpendicular to the peptide backbone which is practically solvent independent. These electrostatic interactions are, however, absent from the antagonist Ala81MBP(74–85), resulting in great flexibility of the side chain of Arg78. Sequence alignment of the two analogues with several species of MBP suggests a critical role for the positively charged residue Arg78, firstly, in the stabilization of the local microdomains (epitopes) of the integral protein, and secondly, in a number of post-translational modifications relevant to multiple sclerosis, such as the conversion of charged arginine residues to uncharged citrullines. Flexible docking calculations on the binding of the MBP(74–85) antigen to the MHC class II receptor site I-A^u using HADDOCK indicate that Gln74, Ser76 and Ser79 are MHC II anchor residues. Lys75, Arg78 and Asp81 are prominent, solvent-exposed residues and, thus, may be of importance in the formation of the trimolecular T-cell receptor–MBP(74–85)–MHC II complex.

Keywords: conformation; docking; major histocompatibility complex; molecular dynamics; myelin basic epitope.

Multiple sclerosis is a chronic inflammatory demyelinating disease of the central nervous system, which is believed to be mediated by autoreactive T cells [1–3]. The activation of resting T cells reacting with antigens of the central nervous system, specifically with the major histocompatibility (MHC)–antigen complex, is thought to be the primary autoimmune event in multiple sclerosis. Myelin basic protein (MBP) represents 5–15% of the peripheral nervous system myelin protein [4] and plays an integral role in the structure and function of the myelin sheath [5,6]. It was the first agent in brain or spinal cord homogenates found to be responsible for experimental allergic encephalomyelitis (an animal model for human multiple sclerosis) [7–9]. Some of the most important functions of MBP are stimulation of phospholipase C activity [10], actin polymerization in conjunction with Ca^{2+}–calmodulin [11], tubulin stabilization [12], and potential regulatory roles as transcription factors [13].

The detailed high-resolution tertiary structure of MBP is not known [14]. The main structural models of this protein date from the 1980s and represent the abstract combination of biochemical data and secondary-structure prediction algorithms [15–18]. The conformation of the first 14 residues of the acetylated N-terminus [19] and the last 17 residues of the MBP have been investigated by NMR [20]. The most sophisticated structural models of the integral protein are those of Stoner [17] and Martenson [18], based on extensive biochemical and secondary-structure data and the recently determined 3D structure by single-particle electron crystallography [21,22]. It was shown that MBP is a C-shaped molecule when adsorbed into a lipid monolayer, comprising five β-sheets and a large proportion of irregular coil.

Correspondence to I. P. Gerothanassis, Department of Chemistry, Section of Organic Chemistry and Biochemistry, University of Ioannina, Ioannina GR-45110, Greece. Fax: + 302651098799, Tel.: + 3026510983397, E-mail: igeroth@cc.uoi.gr

Abbreviations: Me_2SO, dimethyl sulfoxide; MBP, myelin basic protein; MD, molecular dynamics; MHC, major histocompatibility complex; TCR, T-cell receptor.

(Received 28 February 2004, revised 30 June 2004, accepted 1 July 2004)

The lack of a high-resolution structure of MBP means that it is important to investigate the structure of its epitopes, found in segments 1–14, 22–34, 43–68, 67–75, 75–82, 83–96, 90–99, 114–121, 118–131, 125–131, 130–137 and 131–140 [23–26], which have antigenic properties. Characterization of the molecular features of these antigenic sites may provide insights into their immunogenic properties. This would be useful in the design of synthetic peptides and nonpeptide mimetics that can act as vaccines or artificial regulators of the immune response. Linear and cyclic analogues of several MBP epitopes have been synthesized to identify pharmacophoric groups and develop a molecular model, which may be useful in drug design [27–29].

We have focused our studies on the 74–85 segment of guinea pig MBP, Gln74-Lys75-Ser76-Gln77-Arg78-Ser79-Gln80-Asp81-Glu82-Asn83-Pro84-Val85 [MBP(74–85)]. Arg78 is proximal to a triproline Pro99-Pro100-Pro101 segment, which has been suggested to have potential synergestic effects on the entire structure [30]. Furthermore, this dodecapeptide epitope of MBP is a target of the peptidylarginine deiminase action on Arg78, leading to demyelinaton and thus chemical pathogenesis of multiple sclerosis. We examined the structural features of the encephalitogenic agonist epitope MBP(74–85) and the antagonist analogue Ala81MBP(74–85), using detailed NMR and molecular dynamic studies. It is known from spectroscopic studies that MBP is more extensively folded in the presence of lipids or detergents [31–35] than in aqueous solution [31,32]. We therefore investigated solvent-induced structural changes of the peptides in water and Me_2SO, which might be related to the solvent-dependent structural changes in integral guinea pig MBP. Sequence alignment of the two analogues with several MBP species and docking calculations with respect to the MHC II (I-A^u) receptor site are also reported in an effort to elucidate the role of the positively charged residue Arg78 and the effect of the reduction of cationicity of MBP in the triggering of multiple sclerosis. Flexible docking calculations of the MBP(74–85) epitope with the MHC II–I-A^u recognition site are also reported to explore MHC II anchor residues and solvent-exposed residues that may be important for the interaction of the T-cell receptor (TCR) with the bimolecular complex MHC II–antigen [MBP(74–85)].

Materials and methods

Synthesis of peptide analogues of MBP(74–85)

The linear MBP analogues Gln-Lys-Ser-Gln-Arg-Ser-Gln-X-Glu-Asn-Pro-Val, where X = Asp (agonist) or Ala (antagonist), were synthesized using Fmoc/tBu methodology. 2-Chlorotrityl chloride resin and N^{α}-Fmoc amino acids were used for the synthesis as described previously [27–29a]. Peptide purity was assessed by analytical HPLC (Nucleosil-120 C18; reversed phase; 250 × 4.0 mm), MS (fast-atom bombardment, electrospray ionization) and amino-acid analysis [29].

NMR spectroscopy

Preliminary NMR spectra were acquired at 400 MHz using a Bruker AMX-400 spectrometer (NMR Centre, University of Ioannina, Greece). High-field NMR spectra were acquired at 750 MHz using a Bruker Avance 750 spectrometer (Bijvoet Center for Biomolecular Research, Utrecht, the Netherlands). For water suppression, excitation sculpting with gradients was used [36]. Samples of the MBP-(74–85) and Ala81MBP(74–85) analogues were dissolved in Me_2SO-d_6 at 2 mM concentration, and the spectra were recorded at 300 K. Chemical shifts were reported with respect to the resonance of the solvent. The samples in aqueous solution (90% ^1H_2O/10% ^2H_2O, v/v) were prepared for NMR spectroscopy by dissolving the peptide in 0.01 M potassium phosphate buffer (pH = 5.7), containing 0.02 M KCl and 1 mM 2,2-dimethyl-2-silapentanesulfonate as an internal chemical-shift reference. Peptide concentration was usually 4 mM, and the spectra were recorded at 277 K. Trace amounts of NaN_3 were added as a preservative.

NOESY experiments – determination of distance restraints

2D Spectra were acquired using the States-TPPI method for quadrature detection, with 2K × 512 complex data points, 16 scans per increment for 2D TOCSY, and 64 scans for 2D NOESY experiments. The mixing time for the TOCSY spectra was 80 ms. The mixing times for NOESY experiments were 100, 200, 300 and 400 ms. Data were zero-filled in t_1 to give 2K × 2K real data points. A 60 ° phase-shifted square sine-bell window function was applied in both dimensions using the NMRPIPE software [37].

Interproton distances were derived by measuring cross-peak intensities in the NOESY spectra. Intensities were calibrated to give a set of distance constraints using the NMRVIEW software package [38].

Structure calculations

Structure calculations were performed with CNS [39] using the ARIA setup and protocols [40,41], as described in Bonvin *et al.* [42] Covalent interactions were calculated with the 5.3 version of the PARALLHDG parameter file [43] based on the CSDX parameter set [44]. Nonbonded interactions were calculated with the repel function, using the PROLSQ parameters [45] as implemented in the new PARALLHDG parameter file. The OPLS nonbonded parameters [46] were used for the final explicit solvent refinement (water or Me_2SO) including full van der Waals and electrostatic energy terms.

A simulated annealing protocol in Cartesian space was used starting from an extended conformation consisting of four stages: (a) high-temperature SA stage (10 000 steps, 2000 K); (b) a first cooling phase from 2000 to 1000 K in 5000 steps; (c) a second cooling phase from 1000 to 50 K in 2000 steps; (d) 200 steps of energy minimization. The time step for the integration was set to 0.003 ps.

The structures were subjected to a final refinement protocol with the explicit solvent by solvating them with either a 8 Å layer of TIP3P water molecules [46] or a 12 Å layer of Me_2SO molecules [43]. The resulting structures were energy-minimized with 100 steps of Powell steepest descent minimization, and the stereochemical quality was evaluated with PROCHECK [47].

Table 1. Summary of the various MD simulations at 300 K. The simulated time in each case was 10 ns.

Code	Peptide	Solvent	Starting structure
(1)	Agonist	H_2O	Lowest energy NMR structure in H_2O
(2)	Antagonist	H_2O	Lowest energy NMR structure in H_2O
(3)	Agonist	Me_2SO	Lowest energy NMR structure in Me_2SO
(4)	Antagonist	Me_2SO	Lowest energy NMR structure in Me_2SO
(5)	Agonist	H_2O	Lowest energy NMR structure in Me_2SO

Molecular dynamics (MD) simulations

Simulations were performed with GROMACS 3.1 [48,49], using the GROMOS96 43A1 force field [50]. The simulations were run for 10 ns at 300 K starting from the lowest-energy NMR structures, in either explicit water, using the SPC model [51], or Me_2SO, using the model of Liu *et al.* [52] (Table 1). Analysis of the trajectories was performed using the programs included in the GROMACS package.

The peptides were solvated in a cubic box of explicit water or Me_2SO with a minimum distance solute–box of 14 Å. The various systems comprised 3899 and 4516 SPC molecules for the agonist and the antagonist in water, respectively, and 817 and 927 Me_2SO molecules for the agonist and the antagonist, respectively, corresponding to a total number of atoms of 11 797, 13 673, 3398 and 3832, respectively. Periodic boundary conditions were applied. Each system was first energy-minimized using 2000 steps of steepest descent algorithm. For the antagonist, the system was neutralized by replacing a water molecule (with the highest electrostatic potential energy) with a Cl^- counter ion, and then energy-minimized with 2000 steps of steepest descent.

Each system was equilibrated in five 20 ps phases, during which the force constant of the position restraints term for the solute was decreased from 1000 to 0 $kJ{\cdot}mol^{-1}{\cdot}nm^{-2}$ (1000, 1000, 100, 10, 0). The initial velocities were generated at 300 K following a Maxwellian distribution. The simulations were performed at constant pressure (101 kPa) and temperature (300 K) by weakly coupling the system to external temperature and pressure baths [53], except for the first 20 ps equilibration part which was performed at constant volume. All bonds were constrained by using the LINCS algorithm [54], and the water molecules were kept rigid using the SETTLE algorithm [55]. The peptide and the solvent (as well as the counter ion in the case of the antagonist simulations) were coupled separately to a temperature bath with a time constant of 0.1 ps. The pressure was coupled to an external bath at 100 kPa with a time constant of 0.5 ps and a compressibility of 4.5×10^{-3} kPa^{-1}. Periodic boundary conditions were applied all along the simulation. A twin-range cut-off of 0.8 and 1.4 nm was used for the nonbonded interactions. In water, the generalized reaction field [56] was used with a dielectric constant of 54 beyond the 1.4 nm cut-off, whereas in Me_2SO a classical shifting function was used with a cut-off of 1.4 nm. A 2 fs time step was used for the leapfrog algorithm integration.

All simulations were performed in parallel on two processors on a LINUX cluster (1.3 MHz Athlon processors) using the parallel version of GROMACS. As a cost per unit cost indication, 1 ns took about 2.5 h for the simulations in Me_2SO and 14 h for those in water. The average solvent-accessible surface area was calculated from frames taken every 100 ps using the program NACCESS [57].

Sequence alignment

Sequence alignment of the different MBP families for the fragment 74(3)–85(7) was performed with CLUSTALW [58].

Docking calculations

The docking calculations were performed with HADDOCK 1.2 [59] (http://www.nmr.chem.uu.nl/haddock) using the standard protocols. The ambiguous interaction restraints for docking calculations were defined for the P4, P6 and P9 pockets of the peptide-binding groove of the MHC II ($I\text{-}A^u$), based on the interactions derived from the X-ray crystallographic structures of several MHC II–MBP epitope complexes (see discussion below). A total of 1000 rigid-body docking solutions were generated. In addition, for each of the starting conformations, 10 rigid-body trials were performed, and only the best solution based on the intermolecular energy was kept, bringing the total effective docking trials to 10 000. The best 500 solutions sorted according to the intermolecular energy (sum of van der Waals, electrostatic, and ambiguous interaction restraints energy terms) were further subjected to the semi-flexible simulated annealing and Me_2SO refinement as described previously [59]. The solutions were clustered using a 1.0 Å rmsd cut-off criterion and ranked according to their average interaction energies (sum of E_{elec}, E_{vdw}, E_{ACS}) and their average buried surface area.

Results and Discussion

NMR studies

Amino-acid spin systems were identified by locating networks of characteristic connectivities in the 2D TOCSY and NOESY spectra [60].

Qualitative results on the conformational properties of the two peptides can be extracted from the difference of the amide protons (NH) chemical-shift temperature coefficients ($\Delta\delta/\Delta T$) between agonist and antagonist. Exposed NHs typically have coefficients in the range −6.0 to −8.5 $p.p.b.{\cdot}K^{-1}$, and hydrogen-bonded or protected NHs typically have $\Delta\delta/\Delta T$ of −2.0 to +1.4 $p.p.b.{\cdot}K^{-1}$ [61]. In Me_2SO solution, only the NH of Lys75 has a $\Delta\delta/\Delta T$ value characteristic of solvent shielding, while the remaining NH groups have $\Delta\delta/\Delta T$ values < -4.5 $p.p.b.{\cdot}K^{-1}$, indicating their exposure to solvent. From the comparison of $\Delta\delta/\Delta T$ values of agonist and antagonist, it can be concluded that the agonist has a more compact conformation in Me_2SO. $\Delta\delta/\Delta T$ values in aqueous solution are not reported because of the large overlap for the NH resonances.

Chemical-shift differences between MBP(74–85) and Ala81MBP(74–85) of $0.02 < \Delta\delta < 0.04$ p.p.m. were found for Ser76, Gln77, Arg78, Ser79, Asn83 in Me_2SO and aqueous solutions. Larger differences (> 0.05 p.p.m) were observed for Gln80 and Glu82, which are neighbours to the variant position 81. The large deviations for the C-terminal residues Asn83 and Val85 observed in aqueous solution, compared with Me_2SO, are possibly due to electrostatic interactions promoted in this solvent (see discussion below). A comparison of the chemical-shift data of the two peptides suggests that the backbone of the two molecules should exhibit different structural features in both solvents.

Structure determination of MBP(74–85) and Ala81MBP(74–85)

The primary NMR data used in the structure calculations were sequential ($|i–j| < 1$), medium-range ($1 < |i–j| < 4$) and long-range ($|i–j| > 4$) NOEs, obtained from ^{1}H to ^{1}H 2D NOESY experiments. Several NOE connectivities indicative of a folded conformation were observed for the two analogues. For the structure calculations of MBP (74–85) in Me_2SO, 98 sequential and medium-range NOEs and two long-range NOEs were used as distance restraints, whereas, in aqueous solution, 116 sequential and medium-range NOEs and two long-range NOEs were considered. For the structure calculations of the Ala81MBP(74–85) analogue in Me_2SO, 64 sequential and medium-range NOEs were used as distance restraints, and in the case of the aqueous solution, 83 sequential and medium-range NOEs were considered. NOE cross-peaks were separated into three distance categories according to their intensity. Strong NOEs were given an upper distance restraint of 3.0 Å, medium NOEs of 4.0 Å, and weak NOEs of 5.5 Å. The lower distance limits were set to 1.8 Å. No other restraints were applied. Structure calculations were performed using a simulated annealing protocol, following the ARIA/CNS setup [40–42] (see Materials and methods).

Structure in aqueous solution. A family of 200 structures was calculated for both analogues in aqueous solution. The 20 structures with the lowest total energy and NOE violations smaller than 0.25 Å were selected after the final refinement in explicit water. Both the N-terminal and C-terminal regions exhibit significant conformational heterogeneity, whereas the Lys75–Glu82 segment maintains a more consistent conformation (Fig. 1).

The MBP(74–85) epitope adopts a compact, S-shaped, conformation in aqueous solution, with rmsd values from the mean structure for the Lys75–Glu82 fragment of 0.90 ± 0.25 Å for the backbone N, C^{α}, C′ atoms and 2.05 ± 0.55 Å for all heavy atoms. A characteristic feature of this ensemble of structures is the presence of two conformational families with different orientations of the side chain of Glu82. We termed these two families of conformers 1 (#1) and 2 (#2) (Fig. 1A, black and grey backbones, respectively). In family 1 (#1) the side chain of Glu82#1 is in close proximity to Gln77, whereas in family 2 (#2, Glu82#2) it approaches the side chain of Lys75 [this is consistent with the observed long-range NOE cross-peak between Lys75 (Hα) and Arg78 (HN)]. Furthermore, in both families, Glu82 is in close proximity to the side chain of Arg78, forcing it into a perpendicular position relative to the

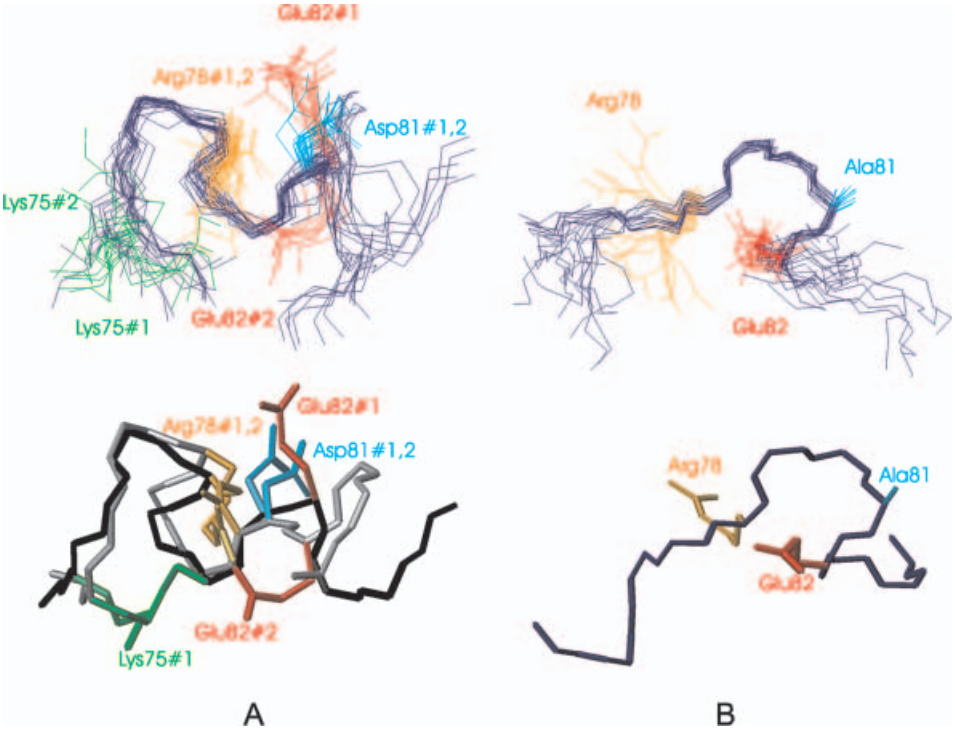

Fig. 1. Ensembles of 3D structures of the agonist (A) and antagonist (B) linear analogues of MBP(74–85) in aqueous solution. The lower thicker trace corresponds to a representative conformer, the structure of which is closest to the average structure of the ensemble.

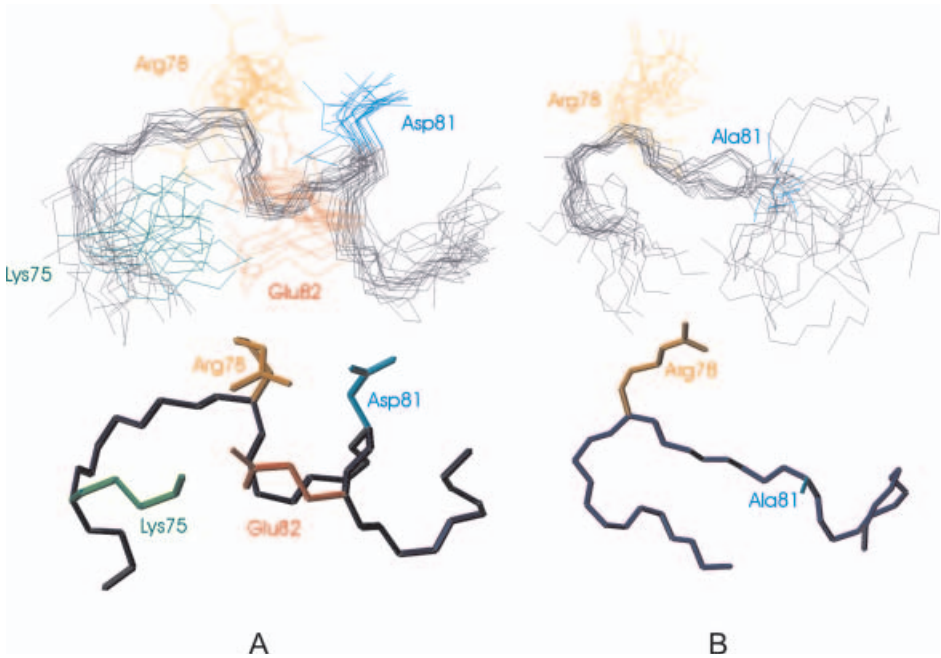

Fig. 2. Ensembles of 3D structures of the agonist (A) and antagonist (B) linear analogues of MBP(74–85) in Me_2SO-d_6 solution. The lower thicker trace corresponds to a representative conformer, the structure of which is closest to the average structure of the ensemble.

plane defined by the backbone of the peptide [this is consistent with the observed two long-range NOE cross-peaks between the side chain of Arg78 (H^{ε}) and Glu82 ($H^{\gamma 1}$ and $H^{\beta 1}$)]. The side-chain carboxylate group of Asp81, is well defined, and it interacts with the side-chain amide proton (Hε) of the neighbouring residue Gln80.

The Ala81MBP(74–85) variant seems to adopt a more open U-shaped loop conformation of residues Arg78–Ala81 (Fig. 1B). The rmsd values from the mean structure for the Lys75–Glu82 fragment are 0.95 ± 0.40 Å and 2.65 ± 0.75 Å for backbone N, C^{α}, C′ atoms and all heavy atoms, respectively. A high degree of conformational heterogeneity can be observed for the side chain of Arg78, in contrast with the native MBP_{74-85} epitope. This can be attributed to the absence of the negative charge at position 81. This is an important structural feature that discriminates the agonist encephalitogenic MBP(74–85) epitope from the antagonist analogue Ala81MBP(74–85) (see discussion below).

Structure in Me_2SO solution. As was the case for the aqueous solution, the 20 structures of the two peptides with the lowest total energy and NOE violations smaller than 0.25 Å were selected after the final refinement in Me_2SO. The N-terminal and C-terminal regions exhibit conformational heterogeneity (especially in the case of the antagonist analogue), whereas the Lys75–Glu82 segment maintains a more consistent conformation.

The MBP(74–85) epitope adopts a quite compact conformation (Fig. 2A), with rmsd values from the mean structure for the Lys75–Glu82 fragment of 1.05 ± 0.40 Å and 2.05 ± 0.60 Å for backbone N, C^{α}, C′ atoms and all heavy atoms, respectively. As was the case in water, the key characteristic of the structure of the native epitope in Me_2SO is the presence of a large number of electrostatic interactions, especially in the central region of the peptide. The side chain of Arg78 is locked into a conformation resembling its conformation in aqueous solution, i.e. perpendicular to the plane defined by the backbone of the peptide. The origin of this structural orientation in Me_2SO is also the strong electrostatic interactions of the side chain of Arg78 with the side chains of Asp81 and Glu82 [this is consistent with the observed long-range NOE cross-peak between the side chain of Arg78 (H^{η}) and Glu82 ($H^{\gamma 1}$) and the medium-range NOE between the side chains of Asp81 (H^{β}) and Arg78 (H^{η} and H^{γ})]. In addition, Glu82 interacts with the side chain of Lys75.

The Ala81MBP(74–85) antagonist in Me_2SO adopts a less compact conformation than the MBP(74–85) epitope (Fig. 2B). The rmsd values from the mean structure for the Lys75–Glu82 fragment are 1.90 ± 0.55 Å and 3.40 ± 0.80 Å for backbone N, C^{α}, C′ atoms and all heavy atoms, respectively. The C-terminal part (Ala81–Val85) appears to be much more flexible, with Ala81 far distant from the side chain of Arg78. The side chain of Arg78 is less well defined, as in the case of aqueous solution, because of the absence of interactions with the side chains of Asp81 (in the agonist analogue) and Glu82.

MD simulations of MBP(74–85), and Ala81MBP(74–85) in water and Me_2SO

To further assess the structural origin of the difference in activity between the agonist and antagonist, their dynamic behaviour was investigated in detail by MD simulations in a specific solvent (Me_2SO and water) [62]. Five 10 ns MD simulations starting from various structures in either Me_2SO or water were performed (Table 1). The evolution of the radius of gyration, which reflects the compactness of

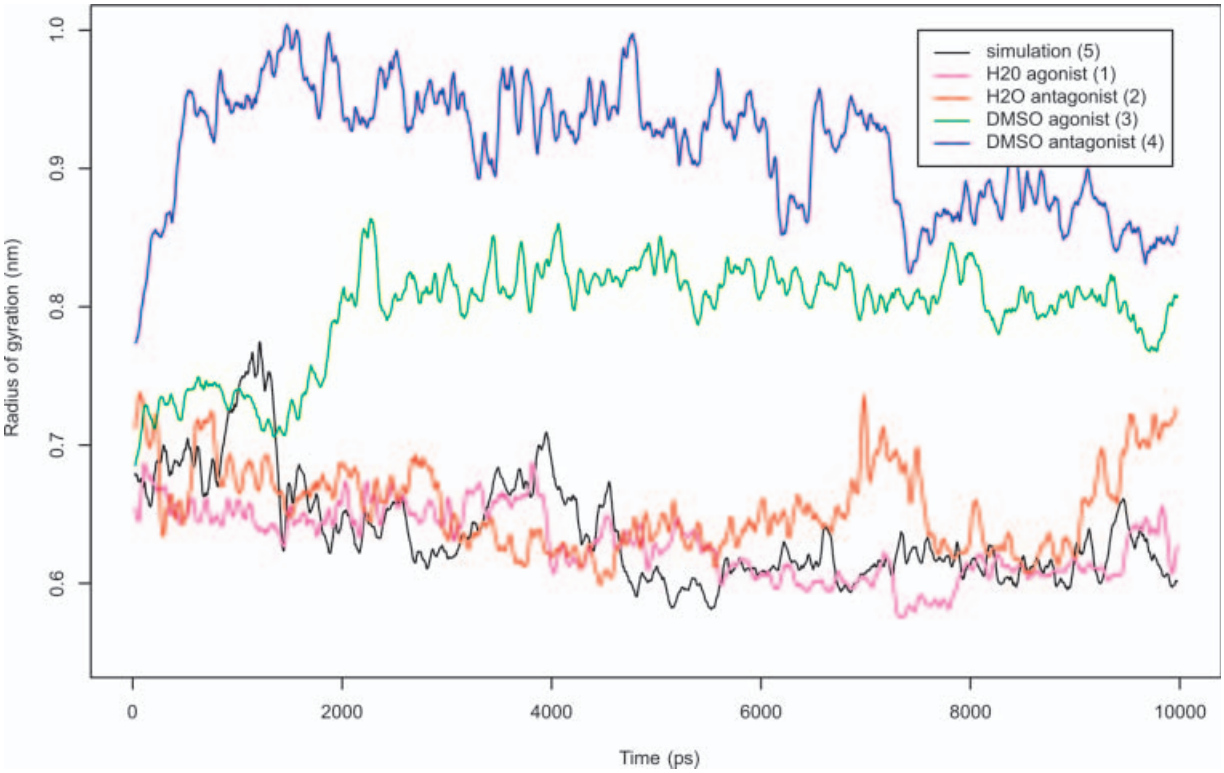

Fig. 3. Evolution of the radius of gyration of the MBP(74–85) and Ala81MBP(74–85) peptides for the five MD simulations of Table 1.

the molecule, is presented as a function of time in Fig. 3. The peptides adopt more extended conformations in Me_2SO than in water. The agonist in Me_2SO is more compact than the antagonist, in agreement with the NMR data. In water, however, no conclusion can be drawn because we cannot distinguish any statistically relevant differences, and longer simulation times would be required for comparison with NMR data. Interestingly, various turn structures (type I′ β, type II and one turn of an α-helix) are observed in various simulations for the segment Arg78-Ser79-Gln80-Asp81.

The cross rmsd matrix in Fig. 4 allows us to compare the different trajectories. The pairwise backbone rmsd values are colour-coded from 0.15 nm (blue) to 0.88 nm (red). As already revealed by the gyration radius (Fig. 3), the cross rmsd matrix clearly shows that the structures in Me_2SO and water are different (yellow–orange off-diagonal blocks between the simulations in water and Me_2SO). Further, the differences between the agonist and the antagonist are somewhat larger in water than in Me_2SO. At 8 ns in water, the antagonist seems to move towards a conformation that is closer to the conformation of the agonist. In Me_2SO, the differences are less important. Trajectory 5 shows the case of the agonist in water starting from the NMR structure in Me_2SO; it can be seen that the starting structure disrupts very quickly and moves towards the conformation of the agonist in water [blue off-diagonal blocks between simulations (1) and (5)].

As mentioned previously, Arg78 is of particular interest as it is the target of various post-translational modifications that might lead to demyelination. Therefore, particular attention was paid to the dynamic behaviour of its side chain, as well as to its interactions with other charged groups. Figure 5 illustrates the evolution of some relevant distances between charged groups in water. In the agonist, the side chain of Arg78 is almost always less than 4 Å from a negatively charged group, mainly Asp81 and Glu82, but also the COO^- terminal of Val85. This is definitely not the case for the antagonist, as Arg78 forms a significantly smaller number of interactions. In Me_2SO, the situation is even more striking; in the agonist, the side chain of Arg78 'sticks' tightly to Glu82 during the entire trajectory, and it interacts with Asp81 between 0 and 5 ns. This is further confirmed by the average number of hydrogen bonds of the side chain of Arg78 for the simulations in Me_2SO; the agonist forms a significantly higher number of interactions than the antagonist. For the simulations in water, the differences are not significant enough to draw any conclusion. We can conclude that Arg78 adopts a predetermined geometry in the case of the agonist, which makes it somewhat more accessible than the antagonist, as suggested by the solvent-accessible surface area. These data clearly demonstrate the structural importance of the nature of the amino acid at position 81 of the encephalitogenic sequence 74–85 of guinea MBP: replacement of Asp81 with an alanine seems to break a chain of electrostatic interactions, especially between the side chains of Arg78 and Glu82/Asp81 independently of the nature of the solvent (protic or nonprotic). This might come from the peptide conformation, which drives the orientation of these two side chains and lets them part preventing any interaction.

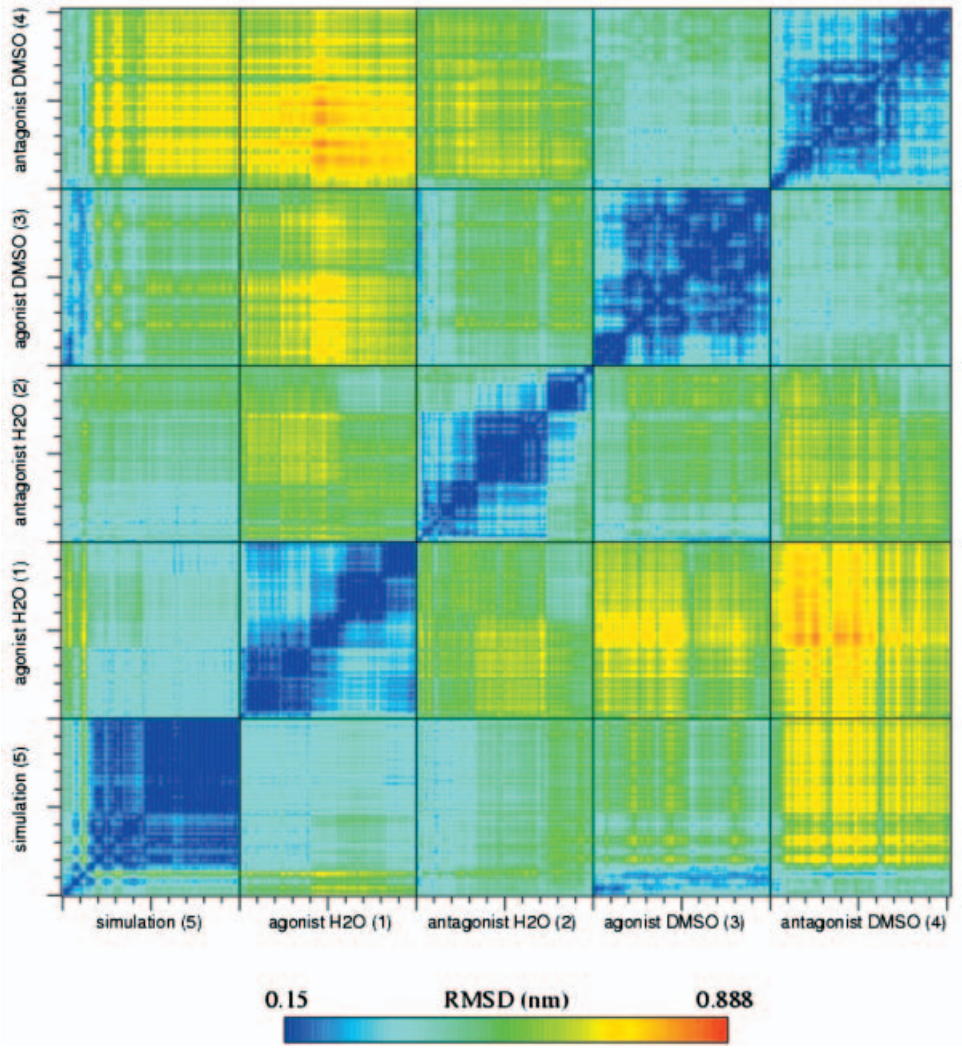

Fig. 4. Backbone cross RMSD matrix for the comparison of the various conformers of the five MD simulations of Table 1. The *x* and *y* axes correspond to the simulation time of the various systems (10 ns each). The rmsd values are colour-coded accordingly to the scale given at the bottom.

Sequence alignment of the MBP(74–85) epitope with the same region of various MBP species

The sequences of several forms of MBP from different species are known [7,8]. The relationship between the amino-acid sequence and immune response has been extensively investigated [2,5]. Differences in the amino-acid sequence of MBP from various animal species have a significant effect on the encephalitogenicity of different determinants from MBP [5]. Sequence alignment of the 74–85 sequence of guinea pig with the same region of MBPs from other species is illustrated in Fig. 6, and reveals that Gln74, Lys75, Ser76, Arg78, Asp81, Glu82, Asn83, Pro84 and Val85 (numbered according to the guinea pig species) are highly conserved. Structure–activity studies have shown that the MBP(74–85) peptide analogue induces experimental autoimmune encephalomyelitis in Lewis rats and that single alanine-substituted peptide analogues at positions Lys75, Ser76, Arg78, Gln80, Asp81, Glu82, and Pro84 resulted in significant reduction of the proliferative responses of a T-cell line specific for the MBP(74–85) peptide [63]. The studied segment of guinea pig MBP(74–85), which lacks the His77–Gly78 segment present in bovine MBP, has been reported to be much more encephalitogenic [5].

The sequence alignment illustrated in Fig. 6 reveals that Arg78 and Asp81 are present in all forms of MBP and are thus probably essential for the structure and function of MBP. As previously reported, aspartic acid at position 82 (81 according to the sequence numbering followed here) may be a critical TCR contact residue for the $V\beta8.2^{+}$ encephalitogenic T cells that predominate in the response of LEW rats to the MBP(74–85) epitope [64]. This may explain the antagonistic properties of the Ala81MBP(74–85) peptide. Interestingly Glu82, which is also a conserved residue, shows some interactions with Arg78 in our NMR and MD simulations. Glu82 may therefore act in the same way as Asp81 to stabilize the specific conformation of Arg78 via an electrostatic interaction.

One of the basic characteristics of MBP is its strong positive net charge, which may have a critical role in the

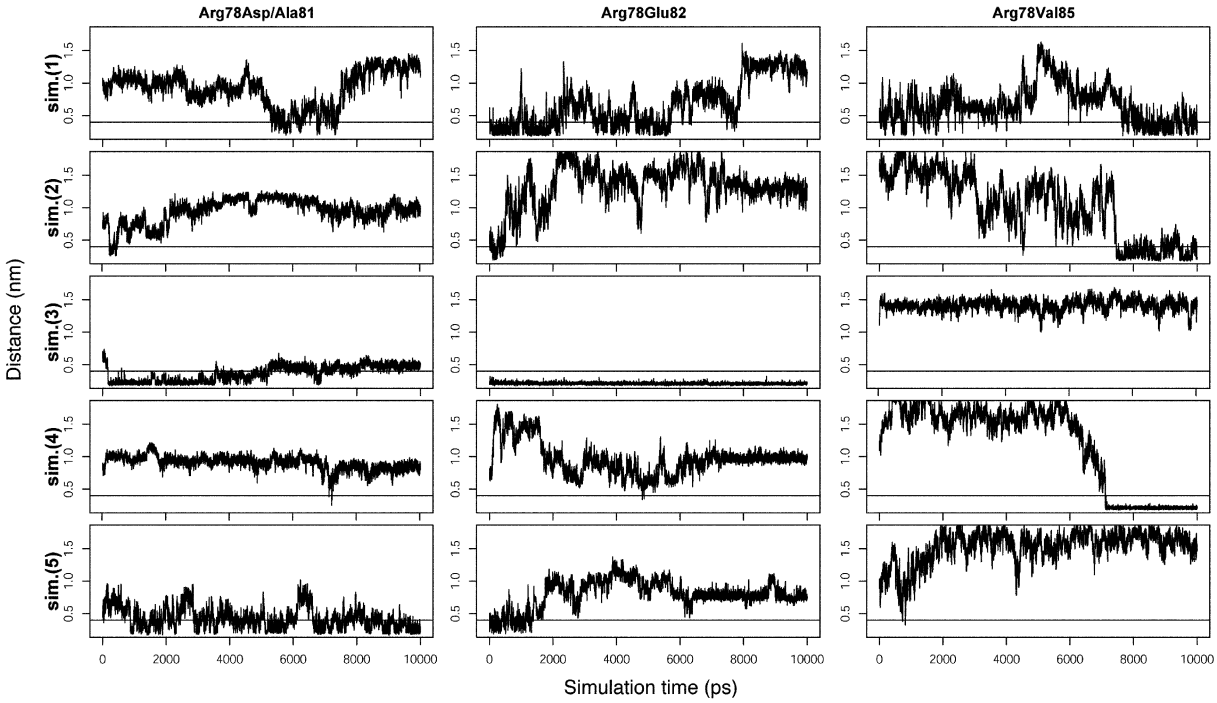

Fig. 5. Evolution of selected distances between charged groups during the five MD simulations.

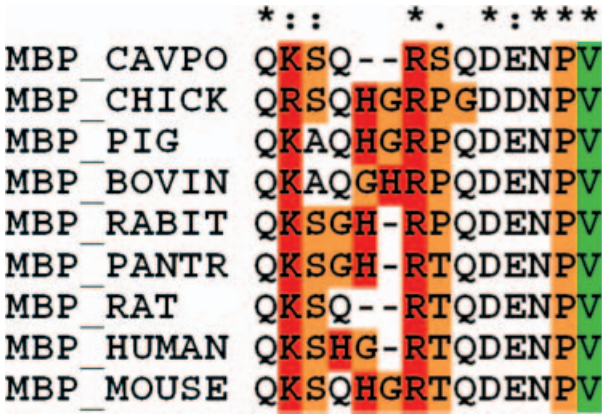

Fig. 6. Sequence alignment of the 74(3)–85(7) segment of MBP_CAVPO [*Cavia porcellus* (guinea pig)], with the same region of MBP_CHICK (chicken), MBP_PIG [*Sus scrofa* (pig)], MBP_BOVIN [*Bos taurus* (bovine)], MBP_RABIT [*Oryctolagus cuniculus* (rabbit)], MBP_PANTR [*Pan troglodytes* (chimpanzee)], MBP_RAT [*Rattus norvegicus* (rat)], MBP_HUMAN [*Homo sapiens* (human)], MBP_MOUSE [*Mus musculus* (mouse)]. The standard colour parameter file of CLUSTALX was used. '*' Indicates positions that have a single, fully conserved residue; ':' indicates that one of the HRK (histidine-arginine-lysine) groups is fully conserved; '.' indicates that one of the STP (serine-threonine- proline) groups is fully conserved.

compaction of myelin, via electrostatic interactions with the cell membrane [65]. It has been suggested [22,25] that the reduction in charge density on citrullinization of arginines (as occurs in multiple sclerosis) diminishes the interaction with negatively charged lipids in the myelin membrane, accounting for a certain amount of destabilization. The role of this strong positive net charge is also important in the MBP epitope studied (Gln74, Lys75, Gln77, Arg78, Gln80, Asn85) in comparison with the more positively charged Ala81 variant. From our studies of the epitope of MBP therefore we may conclude that the conformation of epitopes of the integral protein must be affected by post-translational modifications.

Docking calculations of the MBP(74–85) antigen to the MHC class II receptor site I-A^u – implications for structure–activity relationships

The activation of $CD4^+$ T cells by peptide–MHC complexes is a key event in the induction of autoimmune diseases, such as multiple sclerosis. For a better understanding of the molecular basis of the MBP(74–85) antigen–MHC II recognition, a model for the 3D structure of the MBP(74–85) antigen–MHC II complex is required. The only available structural data are the X-ray crystallographic structures of the bimolecular complexes of the epitopes 1–11, 85–99 and 86–105 with the MHC class II (pdbids: 1fv1, 1bx2 and 1k2d) [66–68]. Superimposition of the above MBP peptides on MHC class II is illustrated in Fig. 7A, and was carried out by superimposing the α1/β1 domains of the MHC class II molecules of the complexes. The main MHC II peptide binding-groove anchor residues of the MBP peptides (P4, P6, P9), as well as important TCR contact residues that are solvent-exposed (P5, P8), superimpose quite well. In addition, the superimposed MBP peptides shown in Fig. 7 are bound in MHC class II molecules of different subclasses and expected to be highly polymorphic in the relevant antigen-binding grooves.

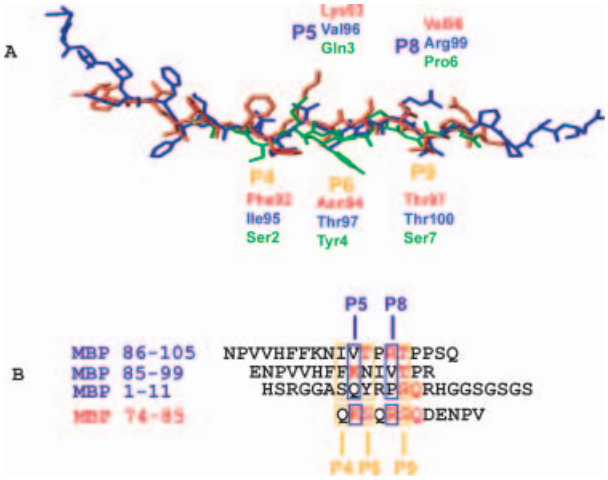

Fig. 7. (A) Superimposition of the MBP (85–99) peptide (red) bound to HLA-DR2b (PDB number 1bx2 [66]) on the MBP(86–105) peptide (blue) bound to HLA-DR2a (PDB number: 1fv1 [67]) and the MBP(1–11) peptide (green) bound to I-A^u (PDB number 1k2d [68]) and (B) sequence alignment of the three antigens derived from the structure alignment. (A) Superimposition was carried out using the α1 and β1 domains of MHC class II molecules. (B) P5 and P8 are prominent, solvent-exposed TCR contact residues of the MBP peptides, and P4, P6 and P9 are MHC II anchor residues of the MBP peptides. Sequence alignment of MBP (74–85) on MHC II binding is also illustrated. Residues conserved among the peptide antigens are indicated in red.

Nevertheless, highly conserved MHC residues exist in the P4, P6 and P9 anchoring pockets [N62α/N62α, Y13β/F11β (F11β points towards Y13β superimposed on DR2 and I-A^u) and Y26β/Y26β form the P4 pockets; N62α/N62α, V65α/T65α and Y13β/F11β form the P6 pockets; N69α/N69α, I72α/V72α, D57β/D57β and Y60β/Y60β form the P9 pockets of DR2/I-A^u]. Sequence alignment of the three antigens derived from the structure alignment and sequence alignment of MBP(74–85) on MHC II binding to the three antigens is illustrated in Fig. 7B (residues conserved among the peptide antigens are indicated in red). The alignment of MBP(74–85) was performed based on the highest aligned score with the three antigens, on the basis of the amino-acid preference for the P4, P6 and P9 MHC II anchor residues and biological experiments in the literature [64]. Interestingly, a statistically significant number of positively charged residues (His, Arg and Lys) were found to project outside the MHC binding groove in the X-ray structures of MHC II–peptide complexes and, thus, may be readily accessible for TCR recognition (Table 2) [66–72].

The sequence of peptide-binding motifs of several MBP peptides and their capacity to bind to MHC class II are illustrated in Table 3. Evidently, there is a preference for serine or threonine as an anchor point for position P9 of the MBP peptide-binding grooves. Interestingly, truncation of the C-terminus of the MBP(86–105) peptide to P9 Thr greatly diminished binding, whereas truncation to P10 Pro had little effect [73,74]. Biological data for the I-A^u–MBP (1–11) complex further support this hypothesis, as deletion of Ser7 of MBP (from the P9 pocket) greatly reduces the affinity of I-A^u for the MBP(1–6) epitope, but substitution with Thr maintains the interaction [68]. This is in accordance with the high conservation of the P9 pocket in the DR2 and I-A^u MHC II molecules, as reported above. The general peptide-binding motifs proposed for MHC class II molecules define amino-acid preferences at positions P1, P4, P6 and P9 [75]. Vogt *et al.* [73] found that MHC II requires an aliphatic residue (valine, isoleucine, methionine or glutamine) at P4 as a main anchor point. As shown in Fig. 7, the sequence alignment of MBP(74–85) with the three antigens fulfil the above amino-acid preferences for the MHC II anchor positions P4, P6 and P9 and show the highest alignment similarity to the MBP(85–106) antigen. Moreover, previous studies have shown that MHC molecules can impose different alignments and conformations on the same bound peptide, as a consequence of topological differences in their peptide-binding sites [67]. Flexible docking calculations using HADDOCK [59] were performed for the docking of the MBP(74–85) epitope to the I-A^u-binding pocket of the immunodominant MBP(1–11) self-peptide [Protein Data Bank (PDB) number 1k2d] [68]. We used the specific MHC, as it has been shown that cryptic epitopes [76,77] within the MBP sequence could, in principle, compete with the immunodominant Ac1–11 epitope for binding to I-A^u [77]. The docking studies were focused on

Table 2. Positively charged residues of bound peptides which are exposed from the peptide-binding groove of MHC II of X-ray structures of MHC II–peptide complexes. Single letter code is used for amino acids.

Peptide bound to MHC II	Exposed residues	Brookhaven PDB code
Human myelin basic protein epitope MBP(85–99) [66]	H90, K93, R99	1BX2
Human myelin basic protein epitope MBP(86–105) [67]	H90, K93, R99	1FV1
Influenza virus haemagglutinin peptide HA(126–138) [69]	H126, H137	2IAD
CLIP fragment (87–101) [70]	K90, R92	1A6A
Endogenous peptide A2(103–117) [71]	R108, R111, H114	1AQD
Ovalbumin peptide OVA (323–339) [72]	H328, H331	1IAO

Table 3. Sequence peptide-binding motifs of several MBP peptides and their binding capacity to the MHC class II receptor site (I-A^u). Only the amino acids of the relevant epitopes involved in the binding of the P1 to P10 MHC pockets are shown. MBP 18 and MBP 21 are derivatives of MBP and defined as described by Garcia *et al.* [68]. ND, Not determined. P4, P6 and P9 (indicated in bold) represent MHCII anchor residues.

	P1	P2	P3	**P4**	P5	**P6**	P7	P8	**P9**	P10	Binding capacity (IC_{50} nM)
MBP(1–11) [67]			A	**S**	Q	**K**	R	P	**S**	Q	70
MBP21 [67]		G	A	**S**	Q	**Y**	R	P	**S**	Q	8.3
MBP18 [67]	R	S	H	**G**	K	**Y**	L	A	**T**	A	15
MBP(85–99)	V	H	F	**F**	K	**N**	I	V	**T**	P	ND
MBP(86–105)	F	K	N	**I**	V	**T**	P	R	**T**	P	ND
MBP(74–85)				**Q**	K	**S**	Q	R	**S**	Q	ND

Table 4. Residues used in the definition of the ambiguous interaction restraints for the flexible docking calculations for I-A^u and MBP(74–85) epitope using HADDOCK [59]. The ambiguous interaction restraints are defined between any atom of the MBP(74–85) listed residue and any atom of the corresponding listed I-A^u residues. The effective distance is calculated by sum averaging over all individual distances (see [59] for details). Single letter code is used for amino acids.

MBP(74–85)	I-A^u
Q74	Y9α, F11β, P13β, Y62β
S76	N62α, T65α, F11β, Y30β
S79	H68α, N69α, V72α, D57β, Y61β

the binding grooves P4, P6 and P9, which were used as restraints, so as to examine the possible structural rearrangement of the residues at positions 78 (lysine) and 81 (arginine), which are highly conserved in all species for the relevant MBP fragment (Fig. 6). All the restraints used in the docking calculations are shown in Table 4.

The molecular model of the I-A^u–MBP(74–85) complex [MBP(74–85) shown in orange] generated with HADDOCK superimposed on the X-ray crystallographic structure of the I-A^u–MBP(1–11) complex [MBP(1–11) shown in blue] is shown in Fig. 8. The peptide groups of MBP(74–85) occupying pockets P4–P10 of I-A^u superimposed quite well on the relevant peptide groups of the MBP(1–11) epitope. Compared with other peptides bound to class II molecules, the C-terminal part of MBP(74–85) is positioned higher in the I-A^u binding groove, like the C-terminus of MBP(85–99) in the HLA-DR2a complex and the MBP(86–105) in the HLA-DR2b complex [66,67]. The MBP(74–85) peptide is bound to I-A^u in an extended, type II polyproline conformation, as previously observed in other class II structures. The mode of binding of the MBP(74–85) peptide to I-A^u is determined by the occupied MHC anchor positions at P4, P6, and P9. In HADDOCK, electrostatics is used during the docking and in the scoring. No explicit hydrogen-bonding potential is used because the electrostatics will take care of proper hydrogen bonding. As a result, several hydrogen

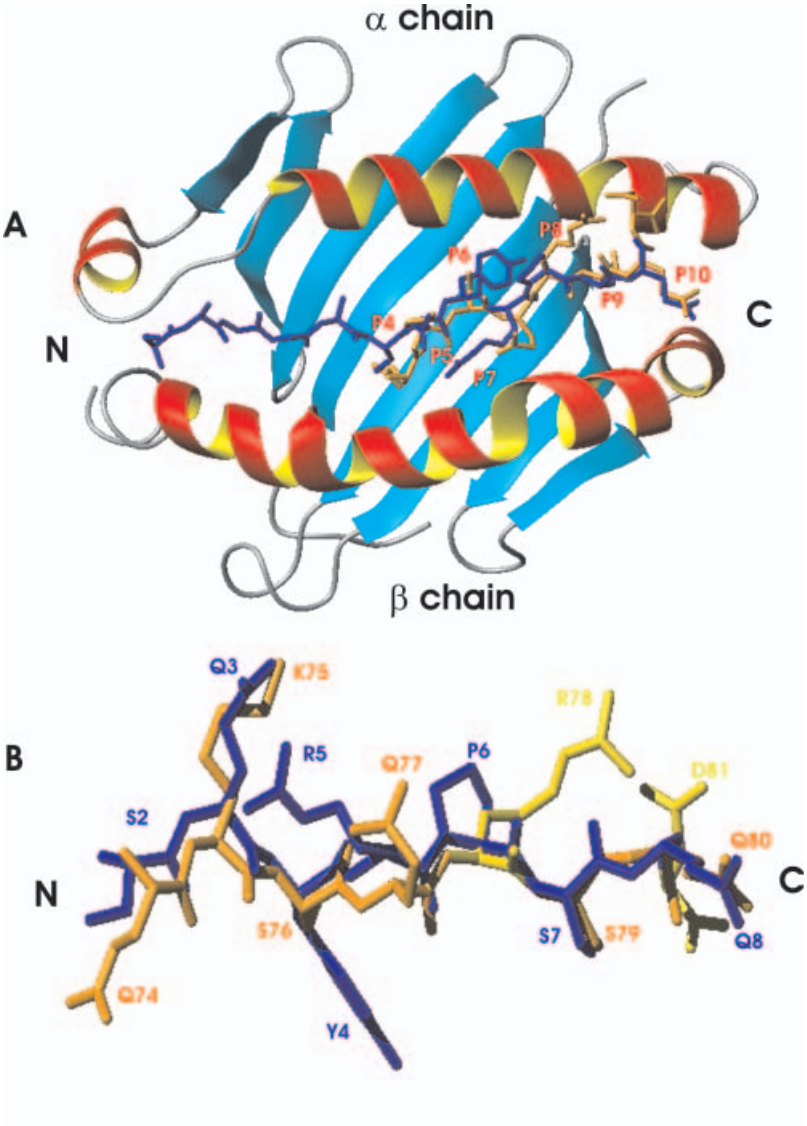

Fig. 8. Superimposition of (A) the X-ray structure of the MBP(1–11) (blue)–I-A^u complex on the model of the MBP(74–85) antigen (orange) complexed to I-A^u obtained by flexible docking with HADDOCK [59] and (B) MBP (1–11) on the MBP(74–85) antigen. Lys75 and Arg78 of MBP(74–85) are prominent, solvent-exposed TCR contact residues. Arg78 and Asp81 (yellow) are probably involved in electrostatic interactions.

Table 5. Intermolecular contacts between I-A^u and MBP(74–85) peptide. Single letter code is used for amino acids.

MBP(74–85)	I-A^u
Hydrogen bonds	
Q74 Oε1	Y9α N
K75 N	E74β Oε2
S76 N	N62α Oδ1
Q77 O	Y61β OH
R78 O	Y66β OH
S79 N	N69α Oδ1
S79 Oγ	N69α Oδ1
van der Waals contacts (< 4.5 Å cut-off)	
Q74	Y9α, F11β, P13β, T28β, Y62β, E74β
K75	F11β, E74β
S76	N62α, T65α, F11β, Y30β
Q77	T65α, N69α, Y30β, Y61β, Y67β
R78	T65α, N69α, H68α, Y61β, Y67β
S79	H68α, N69α, V72α, D57β, Y60β, Y61β
Q80	P56β, Y60β

bonds are formed, which are presented in Table 5. More explicitly, Gln74 occupies the P4 pocket, with a hydrogen bond to Tyr9α N (Gln74 Oε1). The chemical environment of the P6 pocket is a combination of a hydrophobic neck and a moderately hydrophilic base, which favours accommodation of a large, bulky residue in the bound peptide [Tyr4 in the case of the MBP(1–11)]. In the MBP(74–85) epitope, this pocket could accommodate Ser76 which could form a hydrogen bond with Asn62α Oδ1 (Ser76 N) and is in close proximity to residues forming the hydrophobic neck of this pocket (Table 5). The P9 pocket of I-A^u is partially filled by Ser79 similarly to Ser7 of the MBP(1–11) epitope (Fig. 8A,B). This loose fit is compensated for, in part, by a hydrogen bond between Ser79 N and Asn69α Oδ1 and Ser79 Oγ and Asn69α Oδ1. This hydrogen bond is important for the overall I-A^u–MBP stabilization, because deletion of Ser7 of MBP(1–11) greatly reduces the I-A^u affinity for MBP(1–6), but substitution with Thr maintains the interaction [68].

The exposed regions [P5 (Lys75) and P8 (Arg78)] of the peptide point outward and comprise TCR contact residues. In position P8 of the MBP(85–106) and MBP(74–85) epitopes, there is an arginine (Fig. 7A), which in the HLA-DR2a–MBP(85–106) complex is exposed and is a potent TCR contact residue. The relevant arginine (Arg78) of the I-A^u–MBP(74–85) complex was also found to be exposed, in agreement with the NMR and MD structural studies. In addition, Asp81 is also found in an exposed region that is consistent with previous biological experiments, suggesting that this specific residue is a TCR contact residue [64]. A vast body of structural and experimental data [78–80] demonstrates the importance of the P1 anchor for MHC II (I-A^u, I-A^d, I-A^k). We speculate therefore that an extension of the MBP(74–85) epitope in the N-terminus could increase the binding and affinity for I-A^u because of occupation of the P1 pocket.

Recent thermodynamic and kinetic studies of the binding of TCRs to peptide–MHC ligands suggested that the low affinity of the TCR–peptide–MHC complex is a consequence not of insufficient contacts at the interface but, rather, of the entropic penalty associated with the conformational adjustment required for binding [81]. Our studies indicate that the predetermined geometry of Arg78, reduced mobility, and slightly increased average accessible surface area (Fig. 7A) in the case of the agonist peptide result in lower activation energy barriers and smaller conformational adjustments during the TCR–peptide–MHC recognition process.

There is accumulating evidence that epitopes that are similar in sequence and present on viruses and normal human tissue give rise to multiple sclerosis, in which the immune response (T cells or antibodies), directed primarily against the virus, cross-reacts with the human tissue to cause autoimmune disease. An interesting observation is the structural organization of the fragment 76–84 of the Vβ chain of the TCR with specificity for a latent antigen of

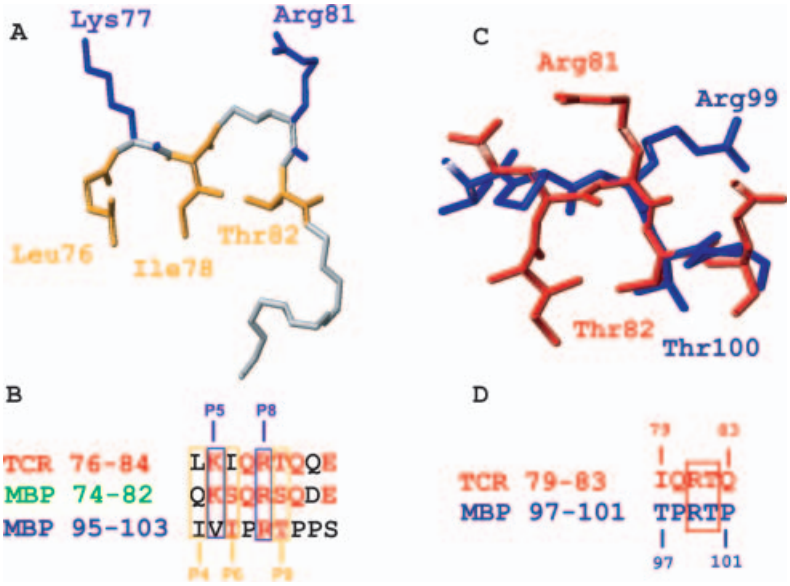

Fig. 9. Structure and sequence alignments. (A) Structure of the 76–82 fragment of the TCR (pdbid: 1kgc) [82] and (B) sequence alignment of the Vβ chain TCR(79–83), MBP(74–85) and MBP(95–103). P5 and P8 are prominent, solvent-exposed TCR contact residues of the MBP(86–105) peptide, and P4, P6 and P9 are MHC II anchor residues of the MBP(86–105) epitope. Residues conserved among the peptide antigens are indicated in red. (C) Superimposition of the MBP(97–101) peptide (blue) bound by HLA-DR2b (PDB number 1fv1 [67]) on the TCR(79–83) fragment (blue). (D) Sequence alignment of the TCR(79–83) fragment and the MBP(97–101) peptide. Residues conserved among the peptide antigens are indicated by a red square.

Epstein–Barr virus [82]. As shown in Fig. 9B, the sequence of the 76–84 fragment of this TCR aligns well with the sequence of both MBP(74–82) (56%) and MBP(95–103) (45%). Interestingly, the structural organization of the 76–84 fragment of this TCR meets the requirements for peptide–MHC II binding, as follows from the conformational reorientation for residues P5 and P8 (exposed) and P4, P6 and P9 (buried) according to the X-ray structure of the MBP(86–102) epitope complexed to MHC II. Figure 9C,D illustrates the structure and sequence alignment of the MBP epitope 97–101 complexed to MHC II and TCR(79–83), focusing on the critical residues arginine and threonine (rmsd 0.27 Å). This provides further evidence for the proposed model of the MBP(74–85) epitope complexed to MHC II.

Conclusions

These NMR, MD and sequence alignment conservation data were obtained to try to identify the microdomain structural organization of critical residues of guinea pig MBP(74–85), which may be involved in triggering multiple sclerosis or affected by post-translational modifications. This local microdomain structural organization may be conserved when the antigen is bound to the MHC II molecule. We focused on Arg78 (a potent target for post-translational modifications) and Asp81 (a TCR contact residue [64]) and found that, in solution, the epitopes studied adopt compact conformations, with a predetermined geometry for the critical residues, i.e. the formation of an Arg78-Asp81 salt bridge in the case of the agonist, which makes it more solvent accessible than the Ala81MBP (74–85) antagonist. Interestingly, this interaction was also found in the MBP(74–85) antigen when bound to MHC II, which adopts an extended, type II polyproline conformation, as revealed by flexible docking calculations. According to biological experiments [64], Asp81 is probably exposed when the MBP(74–85) epitope is bound to I-A^u allowing TCR recognition. As we have identified a direct interaction of this residue with Arg78, it can be expected that this residue is also exposed allowing TCR recognition [P8 MHC II binding pocket in the modelled MBP(74–85)–I-A^u complex].

Our research has shed light on the conformational properties of the guinea pig encephalitogenic epitope MBP(74–85) and the antagonist Ala81MBP(74–85) analogue both in water and Me_2SO solution. Specifically, the study indicates that MBP(74–85) has a compact conformation, with the side chain of Arg78 positioned in a well-defined, predetermined conformation and thus readily accessible for post-translational modifications, which is relevant to multiple sclerosis. This phenomenon is due to the development, in the case of the native epitope, of a network of electrostatic interactions among Lys75, Arg78, Asp81 and Glu82, which results in a bioactive conformation. Although differences were observed in the backbone conformations of the epitope in Me_2SO and aqueous solutions, the conformation of Arg78 is practically solvent independent. Substitution of Asp81 by Ala81 results in high side-chain mobility of the key amino acid Arg78 in both solvents because of the absence of the above interactions.

Sequence alignment of MBP(74–85) with several species of MBP indicates the important role of Arg78, firstly in the stabilization of local microdomains (epitopes) of the integral protein and in a number of post-translational modifications relevant to multiple sclerosis, such as the reduction in cationicity of MBP, especially due to conversion of positively charged arginine residues into uncharged citrulline. In addition, an aspartate residue (81 in the MBP epitope of the guinea pig) is highly conserved in all MBP species, implying a critical functional role previously rationalized to be an important TCR contact residue [64]. The construction of the molecular model of the I-A^u–MBP(74–85) complex through flexible docking calculations and comparison with the HLA-DR2a–MBP(85–106) complex indicate the vital role of Lys75, Arg78 and Asp81 as TCR contact residues.

These results should provide new insights into the molecular mechanism of T-cell activation and be of value in designing experimental autoimmune encephalomyelitis suppressing mimetic analogues with improved pharmacological profile and receptor selectivity.

Acknowledgements

Financial support from the Greek General Secretary of Research and Technology (EPET II 15, PENED 1999) is gratefully acknowledged. The 750 MHz spectra were recorded at the SONNMR Large Scale Facility in Utrecht, which is funded by the 'Access to Research Infrastructures Programme of the European Union' (HPR1-CT-1999-00005). We also thank the SONNMR Large Scale Facility for the use of the computational facilities. Professor H. Kalbacher and Dr V. Apostolopoulos are thanked for useful comments and suggestions. An anonymous referee is greatly acknowledged for his critical comments, which significantly improved the paper.

References

1. Martin, R., McFarland, H.F. & McFarlin, D.E. (1992) Immunological aspects of demyelinating diseases. *Annu. Rev. Immunol.* **10**, 153–187.
2. Steinman, L. (1996) Multiple sclerosis: a coordinated immunological attack against myelin in the central nervous system. *Cell* **85**, 299–302.
3. Ota, K., Matsui, M., Milford, E.L., Mackin, G.A., Weiner, H.L. & Hafler, D.A. (1990) T-cell recognition of an immunodominant myelin basic protein epitope in multiple sclerosis. *Nature (London)* **346**, 183–187.
4. Kursula, P. (2001) The current status of structural studies on proteins of the myelin sheath. *Int. J. Mol. Med.* **8**, 475–479.
5. Deber, C.M. & Reynolds, S.J. (1991) Central nervous system myelin: structure, function, and pathology. *Clin. Biochem.* **24**, 113–134.
6. Kirschner, D.A., Inouye, H., Ganser, A.L. & Mann, V. (1989) Myelin membrane structure and composition correlated: a phylogenetic study. *J. Neurochem.* **53**, 1599–1609.
7. Carnegie, P.R. (1971) Amino acid sequence of the encephalitogenic basic protein from human myelin. *Biochem. J.* **123**, 57–67.
8. Eylar, E.H., Brostoff, S., Hashim, G., Caccam, J. & Burnett, P. (1971) Basic A1 protein of the myelin membrane. The complete amino acid sequence. *J. Biol. Chem.* **246**, 5770–5784.
9. Tompkins, T.A. & Moscarello, M.A. (1993) Stimulation of bovine brain phospholipase C activity by myelin basic protein requires arginyl residues in peptide linkage. *Arch. Biochem. Biophys.* **302**, 476–483.

10. Tompkins, T.A. & Moscarello, M.A. (1994) The mechanism of stimulation of brain phospholipase C-alpha by myelin basic protein involves specific interactions. *Biochim. Biophys. Acta* **1206**, 208–214.
11. Pirollet, F., Derancourt, J., Haiech, J., Job, D. & Margolis, R.L. (1992) Ca(2+)-calmodulin regulated effectors of microtubule stability in bovine brain. *Biochemistry* **31**, 8849–8855.
12. Staugaitis, S.M., Colman, D.R. & Pedraza, L. (1996) Membrane adhesion and other functions for the myelin basic proteins. *Bioessays* **18**, 13–18.
13. Sires, L.R., Hruby, S., Alvord, E.C. Jr, Hellstrom, I., Hellstrom, K.E., Kies, M.W., Martemspm, R., Deibler, G.E., Beckman, E.D. & Casnellie, J.E. (1981) Species restriction of a monoclonal antibody reacting with residues 130–137 in encephalitogenic myelin basic protein. *Science* **214**, 87–89.
14. Sedzik, J. & Kirschner, D.A. (1992) Is myelin basic protein crystallizable? *Neurochem. Res.* **17**, 157–166.
15. Golubovich, V.P., Kirnarskii, L.I. & Galaktionov, S.G. (1989) Theoretical conformational analysis of a encephalitogenic peptide molecule and a study of the structure-activity relationship in a series of its analogs. *Biophysics* **34**, 368–371.
16. Inouye, H. & Kirschner, D.A. (1991) Folding and function of the myelin proteins from primary sequence data. *J. Neurosci. Res.* **28**, 1–17.
17. Stoner, G.L. (1990) Conservation throughout vertebrate evolution of the predicted beta-strands in myelin basic protein. *J. Neurochem.* **55**, 1404–1411.
18. Martenson, R.E. (1981) Prediction of the secondary structure of myelin basic protein. *J. Neurochem.* **36**, 1543–1560.
19. Mendz, G.L., Barden, J.A. & Martenson, R.E. (1995) Conformation of a tetradecapeptide epitope of myelin basic protein. *Eur. J. Biochem.* **231**, 659–666.
20. Price, W.S., Mendz, G.L. & Martenson, R.E. (1988) Conformation of a heptadecapeptide comprising the segment encephalitogenic in rhesus monkey. *Biochemistry* **27**, 8990–8999.
21. Beniac, D.R., Luckevich, M.D., Czarnota, G.J., Tompkins, T.A., Ridsdale, R.A., Ottensmeyer, F.P., Moscarello, M.A. & Harauz, G. (1997) Three-dimensional structure of myelin basic protein. I. Reconstruction via angular reconstitution of randomly oriented single particles. *J. Biol. Chem.* **272**, 4261–4268.
22. Ridsdale, R.A., Beniac, D.R., Tompkins, T.A., Moscarello, M.A. & Harauz, G. (1997) Three-dimensional structure of myelin basic protein. II. Molecular modeling and considerations of predicted structures in multiple sclerosis. *J. Biol. Chem.* **272**, 4269–4275.
23. Fritz, R.B. & Chou, C.H. (1983) Epitopes of peptide 43–88 of guinea pig myelin basic protein: localization with monoclonal antibodies. *J. Immunol.* **130**, 2180–2182.
24. Carnegie, P.R., Dowse, C.A. & Linthicum, D.S. (1983) Antigenic determinant recognized by a monoclonal antibody to human myelin basic protein. *J. Neuroimmunol.* **5**, 125–134.
25. Hruby, S., Alvord, E.C. Jr, Martenson, R.E., Deibler, G.E., Hickey, W.F. & Gonatas, N.K. (1985) Sites in myelin basic protein that react with monoclonal antibodies. *J. Neurochem.* **44**, 637–650.
26. Hruby, S., Alvord, E.C. Jr, Groome, N.P., Dawkes, A. & Martenson, R.E. (1987) Monoclonal antibodies reactive with myelin basic protein. *Mol. Immunol.* **24**, 1359–1364.
27. Tselios, T., Daliani, I., Probert, L., Deraos, S., Matsoukas, E., Roy, S., Pires, J., Moore, G. & Matsoukas, J. (2000) Treatment of experimental allergic encephalomyelitis (EAE) induced by guinea pig myelin basic protein epitope 72–85 with a human MBP (87–99) analogue and effects of cyclic peptides. *Bioorg. Med. Chem.* **8**, 1903–1909.
28. Tselios, T., Daliani, I., Deraos, S., Thymianou, S., Matsouka, E., Troganis, A., Gerothanassis, I., Mouzaki, A., Mavromoustakos, T., Probert, L. & Matsoukas, J. (2000) Treatment of experimental allergic encephalomyelitis (EAE) by a rationally designed cyclic analogue of myelin basic protein (MBP) epitope 72–85. *Bioorg. Med. Chem. Lett.* **10**, 2713–2717.
29. Tselios, T., Probert, L., Daliani, I., Matsoukas, E., Troganis, A., Gerothanassis, I.P., Mavromoustakos, T., Moore, G.J. & Matsoukas, J.M. (1999) Design and synthesis of a potent cyclic analogue of the myelin basic protein epitope MBP72-85: importance of the Ala81 carboxyl group and of a cyclic conformation for induction of experimental allergic encephalomyelitis. *J. Med. Chem.* **42**, 1170–1177.

29a. Tselios, T., Apostolopoulos, V., Daliani, I., Deraos, S., Grdadolnik, S., Mavromoustakos, T., Melachrinou, M., Thymianou, S., Probert, L., Mouzaki, A., Matsoukas, J. (2002) Antagonistic effects of human cyclic MBP_{87-99} altered peptide ligands in experimental allergic encephalomyelitis and human T-cell proliferation. *J. Med. Chem.* **45**, 275–283.

30. Lees, M.B. & Brostoff, S.W. (1984) Proteins of myelin. In *Myelin*, 2nd edn (Morell, P., ed.), pp. 197–224. Plenum Press, New York.
31. Smith, R. (1992) The basic protein of CNS myelin: its structure and ligand binding. *J. Neurochem.* **59**, 1589–1608.
32. Stuart, B.H. (1996) A Fourier transform infrared spectroscopic study of the secondary structure of myelin basic protein in reconstituted myelin. *Biochem. Mol. Biol. Int.* **38**, 839–845.
33. Deibler, G.E., Stone, A.L. & Kies, M.W. (1990) Role of phosphorylation in conformational adaptability of bovine myelin basic protein. *Proteins* **7**, 32–40.
34. Ramwani, J.J., Epand, R.M. & Moscarello, M.A. (1989) Secondary structure of charge isomers of myelin basic protein before and after phosphorylation. *Biochemistry* **28**, 6538–6543.
35. Keniry, M.A. & Smith, R. (1981) Dependence on lipid structure of the coil-to-helix transition of bovine myelin basic protein. *Biochim. Biophys. Acta* **668**, 107–118.
36. Hwang, T.L. & Shaka, A.J. (1995) Water suppression that works. Excitation sculpting using arbitrary waveforms and pulsed field gradients. *J. Magn. Reson. A* **112**, 275–279.
37. Delaglio, F., Grzesiek, S., Vuister, G.W., Zhu, G., Pfeifer, J. & Bax, A. (1995) NMRPipe: a multidimensional spectral processing system based on UNIX pipes. *J. Biomol. NMR* **6**, 277–293.
38. Johnson, B.A. & Blevins, R.A. (1994) Nmrview: a computer-program for the visualization and analysis of NMR data. *J. Biomol. NMR* **4**, 603–614.
39. Brunger, A.T., Adams, P.D., Clore, G.M., DeLano, W.L., Gros, P., Grosse-Kunstleve, R.W., Jiang, J.S., Kuszewski, J., Nilges, M., Pannu, N.S., Read, R.J., Rice, L.M., Simonson, T. & Warren, G.L. (1998) Crystallography & NMR system: a new software suite for macromolecular structure determination. *Acta Crystallogr. D* **54**, 905–921.
40. Linge, J.P. & Nilges, M. (1999) Influence of non-bonded parameters on the quality of NMR structures: a new force field for NMR structure calculation. *J. Biomol. NMR* **13**, 51–59.
41. Nilges, M. & O'Donoghue, S.I. (Year?) Ambiguous NOEs and automated NOE assignment. *Prog. Nucl. Magn. Reson. Spectrosc.* **32**, 107–139.
42. Bonvin, A.M., Houben, K., Guenneugues, M., Kaptein, R. & Boelens, R. (2001) Rapid protein fold determination using secondary chemical shifts and cross-hydrogen bond ^{15}N–$^{13}C'$ scalar couplings (3hbJNC′). *J. Biomol. NMR* **21**, 221–233.
43. Linge, J.P., Williams, M.A., Spronk, C.A., Bonvin, A.M. & Nilges, M. (2003) Refinement of protein structures in explicit solvent. *Proteins Struct. Funct. Genet* **50**, 496–506.
44. Engh, R.A. & Huber, R. (1991) Accurate bond and angle parameters for X-ray protein-structure refinement. *Acta Crystallogr. A* **47**, 392–400.
45. Hendrickson, W.A. (1985) Stereochemically restrained refinement of macromolecular structures. *Methods Enzymol.* **115**, 252–270.

46. Jorgensen, W.L. & Tirado-Rives, J. (1988) The OPLS force field for proteins. Energy minimizations for crystals of cyclic peptides and crambin. *J. Am. Chem. Soc.* **110**, 1657–1666.
47. Laskowski, R.A., Macarthur, M.W., Moss, D.S. & Thornton, J.M. (1993) Procheck: A program to check the stereochemical quality of protein structures. *J. Appl. Crystallogr.* **26**, 283–291.
48. Berendsen, H.J.C., van der Spoel, D. & van Drunen, R. (1995) GROMACS: a message-passing parallel molecular dynamics implementation. *Comp. Phys. Commun.* **91**, 43–56.
49. Lindahl, E., Hess, B. & van der Spoel, D. (2001) GROMACS 3.0: a package for molecular simulation and trajectory analysis. *J. Mol. Model.* **7**, 306–317.
50. Daura, X., Mark, A.E. & Van Gunsteren, W.F. (1998) Parameterization of aliphatic CHn united atoms of GROMOS96 force field. *J. Comp. Chem.* **19**, 535–547.
51. Berendsen, H.J.C., Postma, J.P.M., van Gunsteren, W.F. & Hermans, J. (1981) Interaction models for water in relation to protein hydration. In *Intermolecular Forces* (Pullman, B., ed.), pp. 331–342. Reidel, Dordrecht.
52. Liu, H., Muller-Plathe, F. & van Gunsteren, W.F. (1995) A force field for liquid dimethyl sulfoxide and physical properties of liquid dimethyl sulfoxide calculated using molecular dynamics simulation. *J. Am. Chem. Soc.* **117**, 4363–4366.
53. Berendsen, H.J.C., Postma, J.P.M., DiNola, A. & Haak, J.R. (1984) Molecular dynamics with coupling to an external bath. *J. Chem. Phys.* **81**, 3684–3690.
54. Hess, B., Bekker, H., Berendsen, H.J.C. & Fraaije, J.G.E.M. (1997) LINCS: a linear constraint solver for molecular simulations. *J. Comp. Chem.* **18**, 1463–1472.
55. Miyamoto, S. & Kollman, P.A. (1992) SETTLE: an analytical version of the SHAKE and RATTLE algorithms for rigid water models. *J. Comp. Chem.* **13**, 952–962.
56. Tironi, I.G., Sperb, R., Smith, P.E. & van Gunsteren, W.F. (1995) Generalized reaction field method for molecular dynamics simulations. *J. Chem. Phys.* **102**, 5451–5459.
57. Hubbard, S.J., Thornton, J.M. *NACCESS: Computer Program*. Department of Biochemistry and Molecular Biology, University College London.
58. Thompson, J.D., Higgins, D.G. & Gibson, T.J. (1994) CLUSTAL W: improving the sensitivity of progressive multiple sequence alignment through sequence weighting, positions-specific gap penalties and weight matrix choice. *Nucleic Acids Res.* **22**, 4673–4680.
59. Dominguez, C., Boelens, R. & Bonvin, A.M. (2003) HADDOCK: a protein-protein docking approach based on biochemical or biophysical information. *J. Am. Chem. Soc.* **125**, 1731–1737.
60. Wüthrich, K. (1986) *NMR of Proteins and Nucleic Acids*. John Wiley and Sons, Inc, New York.
61. Andersen, N.H., Neidigh, J.W., Harris, S.M., Lee, G.M., Liu, Z.H. & Tong, H. (1997) Extracting information from the temperature gradients of polypeptide NH chemical shifts.1. The importance of conformational averaging. *J. Am. Chem. Soc.* **119**, 8547–8561.
62. Grdadolnik, S.G., Mierke, D.F., Byk, G., Zeltser, I., Gilon, C. & Kessler, H. (1994) Comparison of the conformation of active and nonactive backbone cyclic analogs of substance P as a tool to elucidate features of the bioactive conformation: NMR and molecular dynamics in DMSO and water. *J. Med. Chem.* **37**, 2145–2152.
63. Wauben, M.H., Boog, C.J., van der Zee, R., Joosten, I., Schlief, A. & van Eden, W. (1992) Disease inhibition by major histocompatibility complex binding peptide analogues of disease-associated epitopes: more than blocking alone. *J. Exp. Med.* **176**, 667–677.
64. Smeltz, R.B., Wauben, M.H., Wolf, N.A. & Swanborg, R.H. (1999) Critical requirement for aspartic acid at position 82 of myelin basic protein 73–86 for recruitment of V beta 8.2+ T cells and encephalitogenicity in the Lewis rat. *J. Immunol.* **162**, 829–836.
65. Moscarello, M.A. (1997) Myelin basic protein, the 'executive' molecule of the myelin membrane. In *Cell Biology and Pathology of Myelin: Evolving Biological Concepts and Therapeutic Approaches* (Jurlink, B.H.J., Devon, R.M., Doucette, J.R., Nazarali, A.J., Scheyer, D.J. & Verge, V.M.K., eds), pp. 13–26. Plenum Press, New York.
66. Smith, K.J., Pyrdol, J., Gauthier, L., Wiley, D.C. & Wucherpfennig, K.W. (1998) Crystal structure of HLA-DR2 (DRA*0101, DRB1*1501) complexed with a peptide from human myelin basic protein. *J. Exp. Med.* **188**, 1511–1520.
67. Li, Y., Li, H., Martin, R. & Mariuzza, R.A. (2000) Structural basis for the binding of an immunodominant peptide from myelin basic protein in different registers by two HLA-DR2 proteins. *J. Mol. Biol.* **304**, 177–188.
68. Xiao-Iin He, Radu, C., Sidney, J., Sette, A., Ward, S. & Garcia, K.C. (2002) Structural snapshot of aberrant antigen presentation linked to autoimmunity: the immunodominant epitope of MBP complexed with I-A^u. *Immunity* **17**, 83–94.
69. Hennecke, J., Carfi, A. & Wiley, D.C. (2000) Structure of a covalently stabilized complex of a human Ab-T cell receptor, influenza Ha peptide and MHC class II molecule, Hla-DR1. *EMBO J.* **19**, 5611–5624.
70. Ghosh, P., Amaya, M., Mellins, E. & Wiley, D.C. (1995) The structure of an intermediate in class II MHC maturation: CLIP bound to HLA-DR3. *Nature (London)* **378**, 457–462.
71. Murthy, V.L. & Stern, L.J. (1997) The class II MHC protein HLA-DR1 in complex with an endogenous peptide: implications for the structural basis of the specificity of peptide binding. *Structure* **5**, 1385–1396.
72. Scott, C.A., Peterson, P.A., Teyton & Wilson, I.A. (1998) Crystal structures of two I-A^d-peptide complexes reveal that high affinity can be achieved without large anchor residues. *Immunity* **8**, 319–329.
73. Vogt, A.B., Kropshofer, H., Kalbacher, H., Kalbus, M., Rammensee, H.G., Coligan, J.E. & Martin, R. (1994) Ligand motifs of HLA-DRB5*0101 and DRB1*1501 molecules delineated from self-peptides. *J. Immunol.* **153**, 1665–1673.
74. Wucherpfennig, K.W., Sette, A., Southwood, S., Oseroff, C., Matsui, M., Strominger, J.L. & Hafler, D.A. (1994) Structural requirements for binding of an immunodominant myelin basic protein peptide to DR2 isotypes and for its recognition by human T cell clones. *J. Exp. Med.* **179**, 279–290.
75. Madden, D. (1995) The three-dimensional structure of peptide-MHC complexes. *Annu. Rev. Immunol.* **13**, 587–622.
76. Kumar, V. & Sercarz, E.E. (1993) The involvement of T cell receptor peptide-specific regulatory CD4+ T cells in recovery from antigen-induced autoimmune disease. *J. Exp. Med.* **178**, 909–916.
77. Fairchild, P.J., Pope, H. & Wraith, D.C. (1996) The nature of cryptic epitopes within the self-antigen myelin basic protein. *Int. Immunol.* **8**, 1035–1043.
78. Lee, C., Liang, M.N., Tate, K.M., Rabinowitz, J.D., Beeson, C., Jones, P.P. & McConnell, H.M. (1998) Evidence that the autoimmune antigen myelin basic protein (MBP) Ac1–9 binds towards one end of the major histocompatibility complex (MHC) cleft. *J. Exp. Med.* **187**, 1505–1516.
79. Fremont, D.H., Monnaie, D., Nelson, C.A., Hendrickson, W.A. & Unanue, E.R. (1998) Crystal structure of I-Ak in complex with a dominant epitope of lysozyme. *Immunity* **8**, 305–317.
80. Nelson, C.A., Viner, N.J., Young, S.P., Petzold, S.J. & Unanue, E.R. (1996) A negatively charged anchor residue promotes high affinity binding to the MHC class II molecule I-Ak. *J. Immunol.* **157**, 755–762.

81. Willcox, B.E., Gao, F.G., Wyer, J.R., Ladbury, J.E., Bell, J.I., Jakobsen, B.K. & van der Merwe, P.A. (1999) TCR binding to peptide-MHC stabilizes a flexible recognition interface. *Immunity* **10**, 357–365.
82. Kjer-Nielsen, L., Clements, C.S., Brooks, A.G., Purcell, A.W., McCluskey, J. & Rossjohn, J. (2002) The 1.5 Å crystal structure of a highly selected antiviral T cell receptor provides evidence for a structural basis of immunodominance. *Structure* **10**, 1521–1532.

Supplementary material

The following material is available from http://www.blackwellpublishing.com/products/journals/suppmat/EJB/EJB4274/EJB4274sm.htm.

Appendix S1. Four Tables with the full assignment (^{1}H and ^{13}C) of the two peptides in both Me_2SO and aqueous solution (Tables S1, S2, S3, S4) and Table S5 with the buried residues for three complex MHC II peptides.

Fig. S1. (A) Plot of temperature coefficients $\Delta\delta/\Delta T$ vs. the amino-acid residues of the MBP(74–85) agonist and the Ala81MBP(74–85) antagonist. Differences in experimental HA and HN chemical-shift values (in p.p.m.) between the proton resonances of MBP(74–85) and Ala81MBP(74–85) in aqueous (B) and Me2SO solution (C).

Fig. S2. Occurrences of a type II β turn on the tetrapeptide RSQD segment.

Fig. S3. (A) Average number of hydrogen bonds of the side chain of Arg78 for the agonist and the antagonist in water and Me2SO solutions. (B) Average solvent-accessible surface area (ASA).

Fig. S4. Superimposition of MHC II molecules (A) and MHC II-bound peptides (B). DR2 (PDB number 1fv1)/[MBP(86–105)], I-Au (PDB number 1k2d)/[MBP(1–11)] and DR2 (PDB number 1bx2)/[MBP(85–99)]. Superimpositions were carried out using the α1 and β1 domains of MHC class II molecules.